

NATIONAL ADVISORY COMMITTEE FOR AERONAUTICS

TECHNICAL NOTE 3308

AN EXPLORATORY INVESTIGATION OF SOME TYPES OF AEROELASTIC
INSTABILITY OF OPEN AND CLOSED BODIES OF REVOLUTION
MOUNTED ON SLENDER STRUTS

By S. A. Clevenson, E. Widmayer, Jr.,
and Franklin W. Diederich

Langley Aeronautical Laboratory
Langley Field, Va.



Washington
November 1954

TECHNICAL NOTE 3308

AN EXPLORATORY INVESTIGATION OF SOME TYPES OF AEROELASTIC
INSTABILITY OF OPEN AND CLOSED BODIES OF REVOLUTION
MOUNTED ON SLENDER STRUTS¹

By S. A. Clevenson, E. Widmayer, Jr.,
and Franklin W. Diederich

SUMMARY

Aeroelastic instability phenomena of isolated open and closed rigid bodies of revolution free to move under elastic restraint have been investigated experimentally at low speeds by means of models suspended at zero angles of attack and yaw on slender flexible struts from a wind-tunnel ceiling. Three types of instability were observed - flutter similar to classical bending-torsion flutter, divergence, and an uncoupled oscillatory instability which consists in nonviolent continuous or intermittent small-amplitude oscillations involving only angular deformations. The speeds at which this oscillatory instability starts were found to be as low as about one-third of the speed at flutter or divergence and to depend on the shape of the body, particularly that of the afterbody, and on the relative location of the elastic axis.

An attempt has been made to calculate the airspeeds and, in the case of the oscillatory phenomena, the frequencies at which these instabilities occur by using slender-body theory for the aerodynamic forces on the bodies and neglecting the aerodynamic forces on the struts. However, the agreement between the speeds and frequencies calculated in this manner and those actually observed has been found to be generally unsatisfactory, with the exception of the frequencies of the uncoupled oscillations which could be predicted with fair accuracy. The nature of the observed phenomena and of the forces on bodies of revolution suggests that a significant improvement in the accuracy of analytical predictions of these aeroelastic instabilities can be had only by taking into account the effects of boundary-layer separation on the aerodynamic forces.

¹Supersedes the recently declassified NACA RM L53E07, "An Exploratory Investigation of Some Types of Aeroelastic Instability of Open and Closed Bodies of Revolution Mounted on Slender Struts" by S. A. Clevenson, E. Widmayer, Jr., and Franklin W. Diederich, 1953.

INTRODUCTION

Flutter, divergence, and similar aeroelastic instability problems of wings and tail surfaces have been recognized for a long time. On the other hand, the related problem of aeroelastic instability of bodies of revolution (generally hereinafter referred to simply as "bodies") has become of interest only recently, primarily because only recently have external stores and fuel tanks in the shape of bodies of revolution been carried on high-speed airplanes, and only at high speeds do the aerodynamic forces exerted on bodies at low angles of attack become sufficiently large to give rise to aeroelastic problems.

There are several differences in the aeroelastic instability phenomena of wings and of bodies, that is, in the nature of the motions, in the nature of the aerodynamic forces involved, and in the nature of the resulting phenomena.

The aeroelastic phenomena of wings essentially involve deformations of the wings themselves, whereas those of bodies are very unlikely to involve significant deformations of the bodies and are based, instead, on the deformation of the members supporting the body. For instance, a fuel tank carried on two struts, one behind the other, under a wing, or a ram jet carried similarly on supports above the fuselage can move laterally as a result of the sidewise deflections of both struts in the same direction, and they can be yawed by a deflection of the front strut to one side and of the rear strut to the other. In these two degrees of freedom, classical flutter may occur under the proper circumstances; under other circumstances and involving only the yawing degree of freedom, classical divergence may occur.

The aerodynamic forces on wings at small angles of attack or undergoing oscillations of small amplitude about zero angle of attack can generally be calculated with sufficient accuracy by potential-flow theory; they are linear functions of the angle of attack or the amplitude, respectively, and are not influenced in an essential way by the boundary layer. (Exceptions to this statement are the forces causing such nonclassical instability phenomena as stall flutter, aileron buzz, and wing buffeting.) The aerodynamic forces on bodies of revolution, however, are often essentially determined by the effects of viscous flow. For instance, the lift which is known to exist on bodies at an angle of attack in steady flow is due entirely to these effects, because potential-flow theory predicts zero lift for this case. This lift is often an intrinsically nonlinear function of the angle of attack. (See ref. 1, for instance.) Consequently, the aeroelastic instability phenomena of bodies are more likely to be of a nonclassical type related to stall flutter and similar phenomena than are the aeroelastic instability phenomena of wings.

Two experimental flutter investigations have been made of bodies mounted on wing tips (refs. 2 and 3), but no aeroelastic-instability studies appear to have been made previously of essentially isolated bodies, that is, bodies mounted at some distance from a lifting surface on flexible struts which contribute no aerodynamic forces. Some instances where this problem arises in practice are external stores or tanks carried on struts under the wing and ram jets carried on supports on top of the fuselage. Also, an analysis of the aeroelastic instability of an isolated body may serve to shed some light on the much more complicated problem of aeroelastic instability of a body mounted on a wing tip.

An investigation has therefore been conducted in order to gain some insight into the nature of the instability phenomena of such isolated bodies of revolution. A streamlined body, an open tube, and several bodies consisting of the tube with variously shaped end pieces were suspended from the ceiling of a wind tunnel on struts of several stiffnesses. The closed bodies were intended to simulate external stores or fuel tanks; the open tube, an unfired ram jet. In one series of tests the tube was also mounted on two struts covered by a fairing. The nature of the various types of aeroelastic instability that occurred under various conditions was observed, as were the airspeeds at which they occurred and the frequencies of any oscillations present. All tests were conducted at low speeds (Mach numbers less than 0.5) and with a range of Reynolds number (based on body length) from 1.5×10^6 to 7.1×10^6 .

In an attempt to analyze some of these results, the speed and oscillatory frequency at which various types of aeroelastic instability may occur have been calculated by using slender-body theory for the aerodynamic forces, with certain additional assumptions in the case of the open tube. The derivation of these forces is presented in the appendix of this paper, and the calculations are described therein. The calculated and observed results are compared and discussed.

SYMBOLS

a	ratio of distance of elastic axis of supporting strut system rearward of midpoint of body to one-half length of body; in case of bodies consisting of tube with various end pieces, the midpoint is that of tube, $\frac{2s_1}{L} - 1$
f	frequency of oscillatory instability, cps
f_h	natural lateral bending frequency of body on struts measured in still air, cps

f_{α}	natural frequency of yawing oscillations of body on struts measured in still air, cps
g	structural damping coefficient (see, for example, ref. 4)
h	lateral translation at elastic axis, ft
h_0	amplitude of lateral-translation oscillation, ft
I_{α}	moment of inertia of body about elastic axis of configuration, slug-ft ²
K_h	effective lateral bending spring constant of supports with body mounted, lb/ft
K_{α}	effective yawing spring constant, ft-lb/radian
k	reduced frequency parameter, $L\omega/2v$
l	aerodynamic force per unit length along body, lb/ft
L	length of body (length of tube, in case of bodies consisting of tube with end pieces), ft
M_{α}	aerodynamic moment about elastic axis, ft-lb
m	mass of body, slugs
P	aerodynamic (lateral) force, lb
q	dynamic pressure (at onset of instability, unless specified otherwise), lb/sq ft
q^*	dimensionless dynamic-pressure parameter, $2qV_b/K_{\alpha}$
R	radius of body of revolution, ft
S	dimensionless cross-sectional area of body, $\pi R^2/L^2$
s	coordinate along length of body, measured rearward from nose, ft
s_1	distance from nose of body to elastic axis of support system, ft
s_2	distance from nose of body to center of gravity of body, ft

V_b	volume of body, cu ft
v	speed (at onset of instability, unless otherwise specified), ft/sec
x_α	ratio of distance of center of gravity of body rearward of elastic axis of support system to one-half length of body, $\frac{s_2 - s_1}{L/2}$
α	yawing angle, radians
α_0	amplitude of yawing oscillations, radians
ξ	dimensionless coordinate, s/L
ρ	density of test medium, slugs/cu ft
ρ_0	density of air at standard sea-level condition, 0.002378 slugs/cu ft
σ	dimensionless distance from nose of body to elastic axis, s_1/L
ω	angular frequency of oscillatory instability, radians/sec
ω_α	natural frequency of yawing oscillations of body on struts measured in still air, radians/sec

DESCRIPTION OF TESTS

Apparatus

Wind tunnel.- The tests were conducted in air at variable pressures in the Langley 4.5-foot flutter research tunnel, which is of the closed-(circular) throat single-return type.

Models.- The two basic models, the airfoil-shaped body and the open tube, are shown in figure 1(a). The airfoil-shaped body of revolution is that generated by rotating an airfoil about its chord. The ordinates of the airfoil are twice those of an NACA 65-010 airfoil and are listed in table 1. The open tube consisted of aluminum sheet 1/16 inch thick rolled into a cylinder with a diameter of 6 inches. Various end sections were used in conjunction with the tube to represent closed bodies of

revolution with a cylindrical center section; these end sections are shown in figure 1(b). The open tube and the airfoil-shaped body are shown mounted on their supports in the tunnel in figures 2(a) and 2(b), respectively. (The scales shown in fig. 2 read in inches.)

Strut-support systems.- The models were mounted on one of four sets of supports which consisted of two small-diameter steel rods fixed on one end to a mounting plate, and on the other end to a mounting bar to which the models were bolted. (See figs. 1(a) and 2.) The struts were designed to make the lateral-bending frequency of the bodies about one-half or one-third of the frequency of their yawing oscillation in still air. The natural frequency of the forward and rearward oscillations of the bodies was approximately six times their lateral-bending frequency. The strut diameters and effective spring constants of the support systems comprised by these struts are listed in table 2.

The effective spring constants were obtained from the frequencies f_h and f_α measured in still air and the known masses and moments of inertia by means of the relations

$$K_h = (2\pi f_h)^2 m$$

and

$$K_\alpha = (2\pi f_\alpha)^2 I_\alpha$$

The values of K_h and K_α obtained in this way represent spring constants in the true sense of the word only when $x_\alpha = 0$, because only then are the yawing and sidewise-bending oscillations uncoupled (and even then only if the additional apparent mass of the still air is neglected). The values given in table 2 are averages of the values obtained with different bodies for $x_\alpha = 0$ (except for the values listed for struts A, for which frequency measurements were made for $x_\alpha = 0.10$ and 0.14).

For one series of tests with the open tube, the struts B were covered with a fairing of aluminum alloy $1/32$ inch thick, which extended about 1 inch ahead of the front strut and $1\frac{1}{2}$ inch behind the rear strut and was attached to the struts along their entire lengths but was not attached to the mounting plate or mounting bar. The airfoil obtained in this manner was about $3/16$ inch thick at and between the two struts, had a rounded leading edge, and a sharp trailing edge.

Strain-gage instrumentation.- The only instrumentation, apart from the usual instrumentation required to measure the tunnel speed and density, consisted of electrical-resistance strain gages mounted on the roots of the struts in such a way as to measure strains due to sidewise deflections of the struts. The output signals of the gages on the front and the rear struts were amplified separately and fed to two channels of a multiple recording oscillograph and also to an oscilloscope for immediate visual observation.

Tests

General procedure.- The procedure for each test was to increase the tunnel speed slowly and at the same time the angle of yaw of the model was adjusted (by yawing the mounting plate by means of a mechanism outside the tunnel) to give zero lift and moment on the body, as indicated by the strain-gage outputs. When some type of instability occurred, the strain-gage outputs were recorded, the type of instability was noted, the tunnel conditions were observed, and the test was discontinued, except in some instances when the instability was not violent and it was desired to study it further.

The model-strut combinations tested in this manner are listed in the left half of table 3; also listed are the model mass, model moment of inertia, elastic-axis and center-of-gravity location, as well as the measured still-air frequencies of each configuration. The tests are divided into several series for the sake of convenience in referring to them.

Tests on the streamlined body.- In series I, the streamlined body was mounted on struts A, the most flexible ones, and the tests were conducted at various air densities. In series II, the same body was mounted on the somewhat stiffer struts B. Only the nonviolent uncoupled oscillatory instability occurred even at the highest air density used in these tests (substantially sea-level density). The tunnel speed was increased successively to several values beyond that at which this instability first occurred, the air density being kept substantially constant at the sea-level value. Test series II consists of measurements of the frequencies of the oscillations at these air speeds. The streamlined body was also mounted on the still stiffer struts C, but no aeroelastic instability of any kind occurred; consequently, this experiment is not listed in table 3.

Tests on the open tube with miscellaneous end sections.- The open tube with various end sections was mounted on struts B, C, and D, that is, on all but the most flexible struts. Series III consists of the tests made with the various configurations at constant air density. Series IV consists of tests made at various densities by using the tube with hemispherical sections at both ends mounted on struts C.

Tests on the open tube on unfaired struts.- Tests made at various air densities on the open tube mounted on the most flexible struts comprise series V, and tests made at constant air densities on the open tube with various center-of-gravity positions mounted on the next stiffer struts comprise series VI. The center of gravity was varied by attaching narrow bands of lead 1/16 inch thick to the inner surface of the tube, so that the mass, the moment of inertia, and, hence, the still-air frequencies were changed as well. The open tube was also mounted on struts D, but no instability occurred at any speed up to and including the speed at which this test was discontinued, namely, 536 feet per second. This test is, therefore, not listed in table 3.

Tests on the open tube on faired struts.- The tests which constitute series VII are those made at constant air density on the open tube mounted on struts B with the fairing attached. The location of the center of gravity was varied in the same manner as in series VI.

RESULTS

Presentation of Results

The results of the tests are presented in the right half of table 3 and some of these results are presented in figures 3 to 9.

The speeds listed in table 3 for tests which led to flutter or divergence are those at which these instabilities first occurred. Similarly, the frequencies listed for the tests which led to flutter are those at the flutter condition. The air speeds listed for the tests of series IV are those observed when the instability first occurred, and the frequencies are those observed at that speed. Similarly, in the tests of series II, the first speed listed is that at which the instability first occurred, but the other speeds are merely speeds above the first at which the frequency of the oscillation was measured. The last speed is that at which the tests of series II were discontinued; the nature of the instability phenomenon did not appear to change in the speed range covered.

The flutter-speed coefficient $2v/L\omega_\alpha$, the dimensionless dynamic pressure at flutter q^* , and the frequency ratio f/f_α pertaining to the tests of series I are plotted in figure 3 against the density ratio ρ/ρ_0 . The frequencies measured in series II are shown plotted as a function of airspeed in figure 4. In figure 5 are shown the speed and dynamic pressure (both in dimensionless form) at the onset of the yawing oscillations observed in the tests of series IV as functions of the density ratio ρ/ρ_0 . The flutter-speed coefficients $2v/L\omega_\alpha$ and the frequency ratios f/f_α pertaining to the tests of series V are shown plotted as functions of the density ratio ρ/ρ_0 in figure 6.

In figure 7 the speed coefficients for which flutter or divergence occurred are shown plotted against x_α for the tests of series VI. The points representing the various tests are not connected because the body mass and moment of inertia (and, hence, the still-air frequencies) were not constant in these tests. Figure 8 consists of a similar plot made for the tests of series VII.

Observed Flutter and Divergence Phenomena

Several types of aeroelastic instability were encountered. In the tests of series I and V, as well as in some of those of series VI and VII, coupled flutter similar to classical bending-torsion flutter was encountered, except that "bending" and "torsion" were lateral motion and yawing, respectively, in the case of these bodies. These two types of motion were distinguished by observing the strain-gage outputs. If the outputs of the front and rear gages had been in phase and of the same magnitude, the motion would have been from side to side only, without yawing, but actually this type of motion was not observed in the tests. When the gage outputs were 180° out of phase and of the same magnitude, the motion was a pure yawing oscillation, and, when they were out of phase by any other angle, the motion was a coupled lateral-motion and yawing oscillation.

In one test of series VII a combined flutter and divergence instability was observed, not unlike the type of phenomenon which a wing may experience if its flutter occurs in a mode which involves very little bending; the tube tended to diverge to the stops after a few oscillations of increasing amplitude. As in all tests where divergence was observed, when the body began to diverge in yaw it moved over laterally as well as under the action of the side forces brought into play by the yawed attitude.

The flutter frequencies were ill-defined occasionally, particularly when the body at its flutter condition was also close to a divergence condition; that is, flutter then occurred so suddenly that no definite frequency could be obtained from the strain-gage record.

Observed Uncoupled Oscillations

An instability was observed in the tests of series II, III, and IV. This phenomenon consisted in continuous or intermittent, self-excited, small-amplitude yawing oscillations, usually with fairly well defined frequency. When the oscillations were intermittent they started up at random intervals rather than subsiding and increasing in a regular fashion, as do oscillations with beats. In two of the tests in which such oscillations occurred the frequency was insufficiently defined to be measured. This phenomenon differed from flutter not only in the fact that it involved small constant amplitudes but also in the fact that, unlike flutter, it involved no bending deformations of the struts and, hence, no lateral

motions of the bodies. For lack of a better name this phenomenon is listed as "yawing oscillations" in table 3 and will be referred to as such hereinafter. If the body were mounted in such a way that the struts were horizontal, as would be the case if a body were mounted on the side of a fuselage, this phenomenon would consist of angle-of-attack or pitching oscillations.

Some of the tests of series III which resulted in yawing oscillations were continued to speeds above that at which the oscillations started; the first speed listed is then the one at which the instability first occurred, and the second is that at which the tests were discontinued. No change was noted in the nature of the phenomenon within this range of speeds. The two frequencies listed for these tests correspond to these two speeds; the values of ρ , q , and q^* are those which correspond to the first speed. In the tests of series III in which no instability occurred, and also in the first test of series VI, the speed listed is that at which the tests were discontinued.

Results of Calculations

Some of the results of the instability calculations described in the appendix are also listed in table 3 and are shown in figures 4, 6, 7, and 8. For series I and II the calculated flutter speed was infinite, that is, the calculations did not predict flutter for any finite speed. Nor was it possible to calculate a finite speed at which self-sustained yawing oscillations could exist, but the frequencies of the yawing oscillations of the body in a moving airstream could be calculated and are shown in table 3 and figure 4.

Flutter speeds and frequencies were calculated for the tests of series V; the results are shown in table 3 and figure 6. Flutter speeds and frequencies as well as divergence speeds were also calculated for the tests of series VI and VII and are listed in table 3; the speed coefficients are also shown in figures 7 and 8.

DISCUSSION

A Note Concerning the Speed and Dynamic-Pressure Parameters

Two dimensionless parameters have been used in order to compare the results of the various tests. The first of these is substantially the one commonly used in flutter work, the flutter parameter or speed coefficient $v/b\omega_\alpha$, where b is the half-chord and is here replaced by one-half the (basic) body length, so that the parameter becomes $2v/L\omega_\alpha$. It involves a measure of the dynamic pressure (in the term v , although the

air density is not taken into account), as well as of the structural and inertia properties involved in angular deformations (combined in the still-air yawing frequency ω_α). The other parameter used herein is one often used in static aeroelastic work and may be referred to as the divergence parameter or dimensionless dynamic pressure; the form of this parameter used in this paper is $q^* = \frac{2qV_b}{K_\alpha}$. It represents the ratio of

the aerodynamic moment per unit angular displacement to the elastic restoring moment per unit displacement and involves implicitly the dynamic pressure as well as the structural and aerodynamic properties pertinent to angular deformation, because the factor 2 is the value of the moment coefficient (referred to the volume of the body) per unit angular displacement according to thin-body theory. This theory applies only to closed bodies, but, if it is extended to open bodies on the basis of the assumption that the flow inside the body has the same velocity as that outside and that the rear end of the body acts like a sharp trailing edge, the same value is obtained for the moment coefficient because the effects of these two assumptions cancel each other.

The main advantage of the flutter parameter is that it includes some dynamic or inertia effects; on the other hand, the advantage of the divergence parameter is that by virtue of its explicit inclusion of aerodynamic properties it serves as a more precise definition of certain instability phenomena. For instance, flutter and divergence can occur over a wide range of values of the flutter parameter, but, although flutter may occur at almost any value of the divergence parameter, divergence should occur at values of this parameter near unity. (If 2 is the correct value of the moment coefficient per unit angular displacement or if the correct value is used in the definition of the divergence parameter instead of 2, divergence will occur when the parameter is 1.) Also, as shown in the appendix, the divergence parameter appears to play an important part in determining the frequency of the uncoupled yawing oscillations.

Both parameters, therefore, have some advantages and, in view of the exploratory nature of the investigation, both have been used in attempts to analyze the observed phenomena.

Flutter and Divergence

Flutter and divergence similar to the classical instability phenomena on wings were both observed on the aerodynamically clean bodies, the streamlined body and the open tube with and without fairing on the struts, as may have been expected, because under certain conditions these bodies have linear aerodynamic forces which may be expected to give rise to phenomena similar to the classical instability phenomena of the wings.

The streamlined body.- The streamlined body fluttered in the tests of series I, in which the density was varied but all other parameters

held constant, at speeds which corresponded to a wide range of the flutter parameter $2v/L\omega_\alpha$ but to values of q^* which varied only between 0.79 and 0.94. The flutter frequency was substantially constant in these tests. (See fig. 3.)

The quantity q^* varied relatively little in these tests because it contains the air density, which was the only variable in these tests. The small variation of q^* in the tests can be considered to be due to the change in the mass ratio, that is, the ratio of the body mass to the mass of the displaced air. Inasmuch as the body would have diverged at $q^* = 1$ if the actual moment on this body in steady flow were that predicted by thin-body theory, flutter occurred in these tests at dynamic pressures from 6 to 21 percent lower than the theoretical dynamic pressure at divergence.

When attempts were made to calculate the flutter speed of the streamlined body, the aerodynamic forces predicted by thin-body theory were found to be incapable of predicting a finite flutter speed. For bodies with a fineness ratio of about 5, the moment due to angle of attack and normal force due to steady rotation predicted by thin-body theory are about 25 and 40 percent higher, respectively, than those predicted by exact potential-flow theory. The values predicted by potential-flow theory are, in turn, somewhat higher than the actual values as the result of boundary-layer separation. Inasmuch as quantitative errors in the predicted forces would tend, by themselves, to result only in an incorrect flutter speed, the fact that the predicted flutter speed does not even exist suggests that aerodynamic forces must be involved which are not predicted by this theory. Such forces are the normal force due to angle of attack and the moment due to steady rotation. These forces are zero according to thin-body and exact potential-flow theory, but actually they do exist; often they vary linearly with angle of attack and rate of rotation, respectively, and thus represent the type of forces required to cause classical flutter.

In the light of this discussion, prediction of the flutter speed of bodies of revolution thus requires a knowledge of the effects of the boundary layer and of the phenomena associated with its separation on the aerodynamic forces. Hence, the main shortcoming of thin-body theory, insofar as the prediction of flutter is concerned, consists in the inability of potential-flow theory in general to predict some of the critical forces involved in these phenomena rather than in the degree to which thin-body theory approximates exact potential-flow theory. In divergence, however, only the moment due to angle of attack is involved; therefore, the correct magnitude of this force is important. Inasmuch as the moment predicted by thin-body theory is about 30 or 40 percent higher than the actual value, the dynamic pressure at divergence would be that much higher than that estimated on the basis of thin-body theory; therefore, in the tests of series I, the highest speed reached probably corresponds to about 80 percent of the true divergence speed.

The open tube on unfaired struts.- In the tests of series V the open tube fluttered at all densities. The values of $2v/La_{\alpha}$ decreased from 10.32 to 5.30 with increasing density, and the values of q^* appeared to increase gradually from 0.516 to 0.579, except for the second test of the series for which q^* was somewhat higher than expected from the other three tests. (See table 3.) These trends are the same as those observed in the case of the streamlined body. In contrast to the streamlined body, however, flutter speeds could be calculated for the open tube on the basis of thin-body theory (with the additional assumptions of unobstructed flow through the tube and of the flow continuing in the same direction after leaving the tail end of the tube rather than reassuming the free-stream direction). These speeds are in fairly good agreement with the measured ones.

The observed frequencies did not vary with the density, a fact which was also noted in the case of the streamlined body. The calculated frequencies did not vary with density either but were about 30 percent higher than the observed ones.

On the basis of these comparisons it appears that the aerodynamic forces are taken into account in a qualitatively correct manner, but that quantitatively they must be improved considerably before they can be used to predict flutter speeds and frequencies correctly for ducted bodies.

In the tests of series VI, the tube fluttered or diverged in all cases, except in the first test, in which the speed of the test was not carried to a high enough value. Flutter occurred when the center of gravity was at or behind the elastic axis, and divergence, when it was at or in front of the elastic axis (see fig. 7); when it was at the elastic axis, the tube fluttered at the higher mass and diverged at the lower mass. This trend agrees with the trends noted in the tests of series I and V, because in these tests there appeared to be a tendency to approach divergence as the air density increased and, hence, the mass parameter decreased. The values of $2v/La_{\alpha}$ at instability varied from 5.47 to 7.95 and those of q^* between 0.459 and 0.754 (see table 3). The values of q^* at divergence tended to be higher than those at flutter, as may be expected in view of the nature of q^* as, primarily, a divergence criterion. No such distinction can be made in the case of the values of $2v/La_{\alpha}$ at instability, both the highest and lowest values of which correspond to divergence.

The calculated speeds at instability are in fairly good agreement with the measured speeds for the rearward locations of the center of gravity, but the flutter speeds predicted for forward center-of-gravity locations are much too low. The two measured flutter frequencies are substantially below the values calculated for those two cases. The calculated divergence speeds are consistently higher than the measured ones by about 20 percent on the average; therefore the moment coefficient per unit angular displacement (the only aerodynamic parameter which enters

the calculation of the divergence speed) must be about 40 percent higher than that estimated by means of the modified thin-body theory used herein. Actually the tube under consideration is not sufficiently slender to justify the use of thin-body theory, and its abrupt changes in cross-section at the nose and tail violate certain assumptions inherent in thin-body theory; also, the validity of the two additional assumptions is doubtful. Hence, the inability of the modified thin-body theory to predict quantitatively useful results is not surprising.

A more accurate potential-flow solution for the flow through and about an open tube would be difficult to obtain, and its validity would still be open to question because the flow inside the tube would be significantly affected by the boundary layer in the inside walls. The available solution for a ring airfoil is inapplicable to this case because the tube is far too slender for this theory. The most promising solution, therefore, appears to be the use of a semiempirical method for estimating the aerodynamic forces required in flutter analysis. Such a method might consist in retaining thin-body theory but modifying the two additional assumptions, that is, by estimating the magnitude of the forces which are, in effect, concentrated at the rear of the afterbody and the extent to which the flow decelerates inside the tubes on the basis of measurements of the moment and normal force due to angular displacement. In divergence calculations only the moment per unit angular displacement is required, of course.

The open tube on faired struts.- The aeroelastic instability phenomena of the tube were substantially unchanged by the addition of the fairing; apparently, the increase in the aerodynamic forces was canceled in effect by the increase in the stiffness of the configuration. Flutter still tended to occur at the further rearward position of the center of gravity, and divergence, at the forward positions. (See table 3 and fig. 8.) The agreement between the calculated and measured speeds was poor, the calculated values being much too low, and the calculated frequency corresponding to the one measured frequency was also much too low. The first two tests of this series serve to illustrate the difficulty of estimating the speed at which aeroelastic-instability phenomena occur; under identical test conditions, the model diverged in one case at 522 feet per second and exhibited some symptoms of flutter at 481 feet per second in the other case, flutter apparently having been suppressed the first time.

The fact that the calculated values of the divergence speed are lower than the observed values indicates that, inasmuch as the aerodynamic moment on the tube due to angular displacement was probably underestimated, as in the tests of series VI, the forces on the fairing were greatly overestimated, as might be expected to be the case because unmodified two-dimensional theory was used to estimate these forces. The exact calculation of the mutual interference effects of the tube and the wing

tip represented by the fairing represents a very difficult problem for which no solution has been found to date. For the time being, therefore, approximations similar to those made herein must be used, although they could probably be improved by resorting to empiricisms based on some measured results.

Yawing Oscillations

The streamlined body; speed at which oscillations start.- When in the tests of series II the streamlined body was tested on stiffer struts and with an elastic-axis location 5 percent of the body length further forward than in the tests of series I, no flutter was observed; instead, the body experienced the self-excited yawing oscillations described previously. These oscillations started at a speed which is relatively low compared to those at which flutter occurred in the tests of series I;

it corresponds to $\frac{2v}{L\omega_\alpha} = 3.76$ and $q^* = 0.211$, and the speed at which

the tests were discontinued corresponds to $\frac{2v}{L\omega_\alpha} = 6.70$ and $q^* = 0.630$,

whereas at the same density flutter would have occurred in the tests of series I at values of $2v/L\omega_\alpha$ and q^* of about 8.0 and 0.9, respectively. Therefore, if the tests of series II had been continued to a speed some 15 or 20 percent higher than that at which they were discontinued, flutter would probably have occurred if the values of $2v/L\omega_\alpha$ and q^* at flutter are assumed not to differ much between the two test series. The fact that oscillations occurred in the tests of series II but not in those of series I is probably the result of the difference in elastic-axis locations, as will be shown later.

In order to calculate the speed at which yawing oscillations might start, an attempt was made to solve the equations of motion for the case of zero lateral displacement. For this case there are two differential equations with one unknown function. With the aerodynamic forces given by thin-body theory, however, the equations can have a solution only when the airspeed is zero. Therefore, the nature of the air forces must again be different from that assumed to yield equations which are compatible at nonzero airspeed.

From a physical point of view, self-excited oscillations can occur only if the net damping is zero. In the equation for the equilibrium of the moments as set up in the appendix, there is no damping term, because the aerodynamic damping moment according to thin-body theory is zero and the structural damping was assumed to be zero. If, however, the aerodynamic moment were actually small and negative, at a certain speed it would be just large enough to counteract the structural damping, and self-excited oscillations would start at this speed. At higher

speeds, the net damping would be negative, but nonlinearities in the aerodynamic forces might prevent the oscillations from diverging. Inasmuch as these aerodynamic forces would then be due entirely to deviation from potential flow, they would probably vary with Reynolds number so that the question whether and when a body might experience self-excited oscillations probably depends on the Reynolds number involved, as well as on the structural damping.

The streamlined body; frequency of oscillations.- Although the equations set up for the analysis of the yawing oscillations do not furnish a solution for the speed at the onset of the oscillations they do give an indication of the frequency of the resulting oscillations, that is, of the "natural" frequency in moving air. This frequency is expressible as a product of the still-air yawing frequency, which involves the dynamic characteristics of the system, and a correction factor which, except for a generally negligible dependence on the mass ratio, is a function only of the static aeroelastic characteristics represented in the parameter q^* , namely $\sqrt{1 - q^*}$. That the trend of the calculated frequencies agrees well with the trend of the frequencies measured for the streamlined body may be seen from figure 4. However, the rate of decrease with speed is less than predicted. This fact suggests that, inasmuch as the expression for the frequency is obtained directly from the equation representing the equilibrium of the moments on the body, the estimated aerodynamic moments on the streamlined body are too large, which is true, as previously noted.

Miscellaneous bluff bodies; effect of elastic-axis location on the speed at which oscillations start.- Yawing oscillations occurred in the majority of the tests of series III. The speeds at which they started correspond to values of $2v/L\omega_{\alpha}$ and q^* much lower than those at which the streamlined body fluttered in the tests of series I and of about the same magnitude as those at which the oscillations of the streamlined body started in series II. (See table 3.) Some of the tests of series III, for instance, the last-listed one, resulted in no instability at what appear to be fairly large values of $2v/L\omega_{\alpha}$ and q^* ; however, all values of $2v/L\omega_{\alpha}$ listed in table 3 are based on the length of the basic tube. If they had been based on the actual lengths of the various bodies, $2v/L\omega_{\alpha}$ would have been about 4 for the last-listed test, which value is about the same as that at which the oscillations of the streamlined body began (3.76) and much lower than that at which that body could have fluttered at this density (about 8). Also, although the value of q^* (0.760) at which this test was discontinued is high compared with that at which the oscillations of the streamlined body started (0.211), it is lower than that at which that body would probably have fluttered at this density (about 0.9). The values of q^* in table 3 for series III are based on the actual volume, as are those for the other series.

The speeds at which oscillations started, in the form of the parameter $2v/L\omega_\alpha$, are shown plotted in figure 9(a) as functions of the dimensionless elastic-axis location a . The importance of the elastic-axis location in determining the speed at which the oscillations start may be deduced from the equation set up in the appendix for the equilibrium of moments in the yawing-oscillations phenomenon, which contains the dimensionless elastic-axis location σ .

In figure 9(a) the upward-pointing arrows on several sketches refer to cases in which no instability was observed; therefore, any instability would have had to occur at values of $2v/L\omega_\alpha$ greater than those shown, which represent those at which these tests were discontinued. Figure 9(a) also contains one point representing the conditions at which the streamlined body started to oscillate in the tests of series II. The sketches in figure 9(a) all imply an airstream approaching from the left.

The only body for which sufficient information was available to deduce the effect of elastic-axis location on the speed at which the oscillations started is the one with hemispherical nose and tail. In figure 9(a) this body is represented by four points which appear to lie on a smooth curve which has a minimum at $a = 0$. For the body with hemispherical nose and streamlined tail, two points were available. These points are connected by a curve based on the pattern exhibited by the body with hemispherical nose and tail which represents the probable variation of the speed coefficient with elastic-axis location, although the minimum of the curve may not be at $a = 0$ as shown. For each of three other bodies (including the body used in the tests of series I and II), one point was available which represented the onset of oscillations and one point which indicated only that the oscillations, if any, would have to start at higher speeds except that, for the streamlined body, the second point represented the flutter condition. Curves representing the estimated variation of speed at the onset of oscillations with elastic-axis location are shown for two of these bodies as well. These approximate curves indicate that the speed at which oscillations start is lowest when the elastic axis is near the midpoint of the body.

By using the estimated variations as a guide, that is, by estimating what the speed would have been if the elastic-axis-location parameter a had been zero, the effect of the body shape on the speed at which oscillations tend to start can be divorced from that of the elastic-axis location.

Miscellaneous bluff bodies; effect of body shape on the speed at which oscillations start.- Inasmuch as a part of the large differences in the speed coefficients shown in figure 9(a) for the various bodies is due to the fact that the coefficients were based on the length of the basic tube, the speed coefficient will be considered to be based on the

actual length of the body in the following discussion. The various bodies then fall into several main classes. Oscillations appear to start at the lowest speeds when the tail of the body is hemispherical, regardless of whether the nose is hemispherical, square (cover plate), or a small cone (for all of which $2v/L\omega_\alpha$ is about 1.3), or a streamlined body (for which $2v/L\omega_\alpha$ is about 1.5). The class with the next highest range of speeds at which oscillations start is that with tails consisting of the streamlined shape or the large cone. If for this group the nose is hemispherical or square, $2v/L\omega_\alpha$ is about 2.5; if the entire body is streamlined, $2v/L\omega_\alpha$ is about 3; and if the nose of the body is a pointed streamlined shape or a large cone, $2v/L\omega_\alpha$ is greater than 4. The class for which oscillations start at the highest speeds is, surprisingly, that with a square tail (cover plate); if for this group the nose is hemispherical or square, $2v/L\omega_\alpha$ is about 3 to 4, and, if the nose is a pointed streamlined shape, $2v/L\omega_\alpha$ is greater than 4. All these numerical values must be used with caution, of course.

In general, then, the speed at which oscillations start appears to depend to a large extent on the shape of the tail of the body, a hemispherical tail being the least favorable in that it oscillates at the lowest speeds, a streamlined tail or large cone used as a tail being much better, and a square tail being most favorable in this respect. The shape of the nose has almost no effect when the tail is hemispherical but has some effect in the other cases, a square or hemispherical nose being worst, a conventionally streamlined (rounded) nose being better, and a pointed streamlined nose, best. The aerodynamically cleanest configuration, the streamlined body, occupies a relatively favorable place; the speed at which it may start oscillating can be increased further by replacing the rounded streamlined nose by a pointed one.

The only way in which the numerical values given for $2v/L\omega_\alpha$ in the preceding discussion can be related to those corresponding to the classical instability phenomena is by noting that the streamlined body fluttered at values of $2v/L\omega_\alpha$ of about 8. As a rule of thumb, then, based on these very limited data, an aerodynamically clean body may be expected to start oscillating at speeds as low as about one-third its flutter or divergence speed. To attempt a similar correlation for bluff bodies would be futile, because these bodies do not experience the linear aerodynamic forces on which the classical instability phenomena are premised.

The reasons for the relative behavior of the various bodies are as yet somewhat obscure. The effects of the nose on the speed at which oscillations start are probably associated with separation at the nose, because the less disturbance caused by the nose, the more favorable the

configuration. Similarly, the behavior of the tail can probably be explained by the effects of separation at or ahead of the tail. The unfavorable effects of the hemispherical tail, for instance, are probably the results of the rather large projected area of the tail (projected on a plane through the axis of the body), which is exposed to the separated flow. The relatively favorable square tail, on the other hand, has no projected area exposed to this flow. The streamlined tail probably causes relatively little separation and thus is relatively favorable if the nose is favorably shaped; this effect corresponds to the observed effects.

In view of the complicated nature of these phenomena there appears to be little hope of arriving at theoretical methods of predicting the speed at which the oscillations start, at least in the case of bluff bodies which are unlikely to be exposed to high-speed airstreams anyway; in the case of more or less streamlined bodies, empirical approaches may prove fruitful. In either case the oscillations do not appear to be violent, and, if they are undesirable, they can always be eliminated by stiffening the supports and in many cases merely by changing the body shape or the elastic-axis location, and possibly also by using vanes mounted on the body.

Miscellaneous bluff bodies; frequency of oscillations.- The ratio of the frequency of the oscillations to those in still air is shown plotted in figure 9(b) as a function of the dimensionless dynamic pressure q^* corresponding to the speed at which the oscillations started. The arrows in figure 9(b) refer to cases in which no frequency was measured and serve merely to call attention to the fact that oscillations did start on the given model at the indicated value of q^* . As in figure 9(a), one point in figure 9(b) represents the conditions at which the streamlined body started to oscillate in the tests of series II. Also, as in figure 9(a), the sketches in figure 9(b) imply an airstream approaching from the left.

The frequencies shown in figure 9(b) agree fairly well with the theoretical curve (which neglects the effect of the mass ratio). In view of the fact that many of the assumptions made in the analysis are violated by the bluff bodies, this agreement is better than may have been expected. All points in figure 9(b) pertain to tests at densities close to sea level. The results of the tests of series IV at various densities follow a similar pattern, although the range of q^* covered by these tests is small. (See fig. 5.) The frequency of the oscillations can thus be estimated on the basis of the relation $\frac{f}{f_\alpha} = \sqrt{1 - q^*}$ with fairly good accuracy. If the body is aerodynamically clean and the speed relatively high, the accuracy of this formula can be improved by replacing the factor of 2 in the definition of q^* by a better value of the moment coefficient per unit angular displacement. At low speeds, the frequency may be expected to be substantially the same as the still-air frequency.

CONCLUSIONS

1. Streamlined bodies and open tubes mounted on thin flexible struts which do not contribute any aerodynamic forces have been found to diverge and flutter; flutter tended to occur for relatively far rearward locations of the center of gravity and for relatively high mass ratios (body mass to mass of displaced fluid).

2. Flutter could not be predicted for the streamlined body by using aerodynamic forces based on potential theory. For the open tube, the calculated flutter and divergence speeds did not agree well with the measured values; the discrepancies are believed to be due to the intrinsic shortcomings of potential-flow theory. The analysis of unsteady aeroelastic effects of bodies of revolution therefore appears to require a knowledge of the boundary-layer and separation effects on the unsteady forces on these bodies.

3. Closed strut-mounted bodies of revolution appear to be subject to a nonclassical instability which consists in self-excited nonviolent oscillations which appear to start, in the case of aerodynamically clean bodies at least, at speeds about one-third that at flutter or divergence for the given body.

4. The speed at which the oscillations start for a given body depends on the elastic-axis location, being lowest when the elastic axis is located near the midpoint of the body. This speed is also determined to a large extent by the shape of the body, particularly of the tail end. For bodies with hemispherical tails, the oscillations start at low speeds but, for bodies with streamlined and, particularly, with squarely cut off tails, they start at relatively high speeds; the optimum nose shape appears to be a pointed streamlined shape and the next best, a conventional streamlined nose shape.

5. The mechanism which causes these oscillations is as yet unknown, although negative aerodynamic damping moments appear to be required. The speed at which the oscillations start cannot, therefore, be predicted at present; its calculation apparently requires a knowledge of boundary-layer and separation effects on the unsteady aerodynamic forces. The frequency, however, can be estimated from a simple formula involving the frequency of the oscillations in still air and the ratio of the given dynamic pressure to that at divergence.

Langley Aeronautical Laboratory,
National Advisory Committee for Aeronautics,
Langley Field, Va., May 12, 1953.

APPENDIX

CALCULATION OF AEROELASTIC INSTABILITIES

Equations of Motion

The equations of motion of a rigid body mounted on flexible supports and performing combined yawing and lateral oscillations are

$$-I_{\alpha}\ddot{\alpha} - m(s_2 - s_1)\ddot{h} - (1 + ig)K_{\alpha}\alpha + M_{\alpha} = 0 \quad (1)$$

$$-m(s_2 - s_1)\ddot{h} - mh\ddot{h} - (1 + ig)K_h h + P = 0 \quad (2)$$

where the dots designate differentiation with respect to time, and where P is the aerodynamic force and M_{α} the aerodynamic moment (positive in the direction of positive h and α , respectively). The manner in which P and M_{α} were calculated for the bodies considered in this paper is described in the following sections.

Aerodynamic Forces on Closed Bodies

The aerodynamic forces on closed bodies of revolution performing unsteady motions in supersonic flow have been calculated by linearized potential-flow theory (see refs. 5 and 6). The aerodynamic forces on bodies of revolution in steady incompressible flow can easily be calculated by potential-flow theory (by using sources and sinks, for instance, as in ref. 7); according to this theory, the normal force is zero. The exact calculation of the aerodynamic force and moment for unsteady motion by potential-flow theory, however, is quite difficult both at subsonic and supersonic speeds, and in view of the fact that they are known to be influenced to a large extent by the effects of viscosity, a large expenditure of effort in calculating them is hardly warranted. In the absence of any means of taking the effects of viscosity into account for unsteady motions, a simple approximation to potential-flow theory, namely slender-body theory, has therefore been used for the purpose of the calculations described herein. (See ref. 8, for instance, for an outline of a slender-body theory in quasi-steady flow.)

The assumption made in slender-body theory is that the momentum of the flow in a plane perpendicular to the free stream is the same as it

would be if this flow were two-dimensional. This assumption implies that the derivative of the radius with respect to distance along the length of the body is small (which implies, in turn, that the body is very slender, that is, the body has a high fineness ratio), and, also, that the angle of attack and any motions are small. (For a fuller discussion of these assumptions from the mathematical point of view, see ref. 9.)

The momentum of the flow about a circular cylinder for a unit length along the cylinder is equal to the product of the rate of motion of the cylinder and the apparent mass, which is equal to the mass of air displaced by a unit length of the cylinder, or $\rho\pi R^2$. At any section of a body of revolution the rate of motion relative to the component of the free-stream velocity normal to the axis of the body is $v\alpha + \dot{h} + (s - s_1)\dot{\alpha}$; this value is within the approximations implied in slender-body theory. Therefore, the momentum per unit length along the body of the flow perpendicular to the body at this section is $\rho\pi R^2(s) [v\alpha + \dot{h} + (s - s_1)\dot{\alpha}]$.

The force exerted by the body on the fluid per unit length along the body is equal to the time rate of change of the momentum per unit length, the rate of change being that along the path of a particle, that is, $\frac{D}{Dt}$. But within the approximation implied in slender-body theory,

$$\frac{D}{Dt} = \frac{\partial}{\partial t} + v \frac{\partial}{\partial x}$$

Therefore, the force per unit length along the body is

$$L = -\left(\frac{\partial}{\partial t} + v \frac{\partial}{\partial s}\right) \left\{ \rho\pi R^2(s) [v\alpha + \dot{h} + (s - s_1)\dot{\alpha}] \right\} \quad (3)$$

Hence, if the body is performing oscillations defined by

$$\alpha = \alpha_0 e^{i\omega t} \quad (4)$$

$$h = h_0 e^{i\omega t} \quad (5)$$

then

$$\begin{aligned}
 l &= -\rho \left(i\omega + v \frac{\partial}{\partial s} \right) \left\{ \pi R^2(s) \left[v\alpha + i\omega h_0 + i\omega(s - s_1)\alpha_0 \right] \right\} e^{i\omega t} \\
 &= -\rho \left\{ \left[2i\omega v \pi R^2(s) - \omega^2(s - s_1)\pi R^2(s) + v^2 \frac{\partial}{\partial s} \pi R^2(s) + \right. \right. \\
 &\quad \left. \left. i v \omega (s - s_1) \frac{\partial}{\partial s} \pi R^2(s) \right] \alpha_0 + \left[-\omega^2 R^2(s)\pi + i v \omega \frac{\partial}{\partial s} \pi R^2(s) \right] h_0 \right\} e^{i\omega t} \quad (6)
 \end{aligned}$$

The aerodynamic force P (positive in the same direction as h) and moment M_α (positive in the same direction as α) are then

$$\begin{aligned}
 P &= \int_0^L l \, ds \\
 &= -\rho V_b \left\{ \left[i\omega v + \omega^2(s_1 - \bar{s}) \right] \alpha_0 - \omega^2 h_0 \right\} e^{i\omega t} \quad (7)
 \end{aligned}$$

and

$$\begin{aligned}
 M_\alpha &= \int_0^L (s - s_1) l \, ds \\
 &= \rho V_b \left\{ \left[v^2 + \omega^2(\bar{s}^2 - 2s_1\bar{s} + s_1^2) \right] \alpha_0 + \right. \\
 &\quad \left. \left[\omega^2(\bar{s} - s_1) + i v \omega \right] h_0 \right\} e^{i\omega t} \quad (8)
 \end{aligned}$$

where

$$\bar{s} = \frac{1}{V_b} \int_0^L s \pi R^2(s) \, ds$$

and

$$\bar{s}^2 = \frac{1}{V_b} \int_0^L s^2 \pi R^2(s) ds$$

or, in dimensionless form,

$$\frac{P}{\rho v^2 L^2 e^{i\omega t}} = - \left[2ikI_0 + 4k^2 (\sigma I_0 - I_1) \right] \alpha_0 - 2k^2 I_0 \frac{2h_0}{L} \quad (9)$$

and

$$\frac{M_\alpha}{\rho v^2 L^3 e^{i\omega t}} = \left[I_0 + 4k^2 (\sigma^2 I_0 - 2\sigma I_1 + I_2) \right] \alpha_0 + \left[ikI_0 + 2k^2 (I_1 - \sigma I_0) \right] \frac{2h_0}{L} \quad (10)$$

where $I_0 = \int_0^1 S(\xi) d\xi$; $I_1 = \int_0^1 \xi S(\xi) d\xi$; and $I_2 = \int_0^1 \xi^2 S(\xi) d\xi$.

For the airfoil-shaped body of revolution, these three values are $I_0 = 0.01626$, $I_1 = 0.00674$, and $I_2 = 0.00335$.

For steady flow ($\omega = 0$) equations (7) and (8) give the known results of slender-body theory:

$$P = 0 \quad (11)$$

$$M_\alpha = \rho v^2 V_b \alpha \quad (12)$$

Aerodynamic Forces on Open Bodies

In attempting to calculate the forces on the open tube in a similar manner, several problems arise. If the recovery factor is assumed to be 100 percent, that is, if the velocity of the flow in the tube is assumed

to be equal in magnitude to the free-stream velocity, the combined apparent mass of both the internal and the external flow at a given section of the body is just twice the apparent mass of the external flow used heretofore. However, one of the assumptions of slender-body theory, namely, the one concerning continuity of the radius along the length of the body, is violated at the nose and tail section of the tube. Consequently, as a result of the abrupt changes in cross-sectional area, not only the concentrated forces predicted by slender-body theory at the nose and tail section but also the distributed forces predicted on the remainder of the tube are open to question.

For lack of a better theory a modified slender-body theory has been used to calculate aerodynamic forces on the open tube. The modification consisted in disregarding the concentrated forces on the tail section on the premise that both the external and the internal flows leave the trailing edge of the tube tangentially and are not realigned with the free stream. This assumption is equivalent to the Kutta condition of subsonic airfoil theory and is used also in the application of slender-body approximation to airfoil theory. (See ref. 10.) The assumption is thus, essentially, that the exit section of the tube acts like the trailing edge of a wing of very low aspect ratio.

With these approximations equations (6), (9), (10), (11), and (12) become, in the case of an open cylindrical tube,

$$z = -2\rho\pi R^2 \left\{ \left[2i\omega v - \omega^2 (s - s_1) + (v^2 - i v \omega s_1) \delta(s) \right] \alpha_0 + \left[-\omega^2 + i v \omega \delta(s) \right] h_0 \right\} e^{i\omega t} \quad (13)$$

where $\delta(s)$ is the delta function which represents the concentrated loads, and

$$\frac{P}{\rho v^2 L^2 e^{i\omega t}} = -2\pi \frac{R^2}{L^2} \left\{ \left[4ik \left(1 - \frac{\sigma}{2} \right) - 4k^2 \left(\frac{1}{2} - \sigma \right) + 1 \right] \alpha_0 + \left(-2k^2 + ik \right) \frac{2h_0}{L} \right\} \quad (14)$$

$$\frac{M_{\alpha}}{\rho v^2 L^3 e^{i\omega t}} = -2\pi \frac{R^2}{L^2} \left\{ \left[2ik(1 - \sigma^2) - \sigma - 4k^2 \left(\frac{1}{3} - \sigma + \sigma^2 \right) \right] \alpha_0 + \left[-2k^2 \left(\frac{1}{2} - \sigma \right) - ik\sigma \right] \frac{2h_0}{L} \right\} \quad (15)$$

$$P_{\omega=0} = -2\rho\pi R^2 v^2 \alpha \quad (16)$$

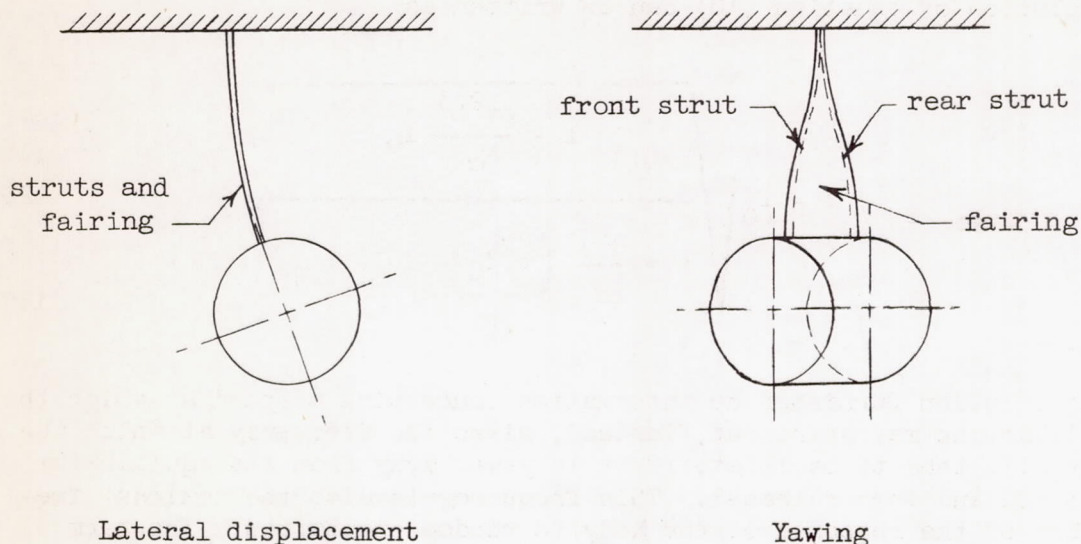
$$M_{\alpha_{\omega=0}} = 2\rho\pi R^2 s_1 v^2 \alpha \quad (17)$$

Calculation of Flutter Speeds and Frequencies

For the streamlined body, the force and moment coefficients given by equations (9) and (10) were introduced into equations (1) and (2) with α and h given by equations (4) and (5), and an attempt was made to solve these equations by the conventional methods of two-degree-of-freedom flutter analysis. (See ref. 4, for instance.) However, no solution was found to exist; therefore, if the aerodynamic forces were correct, the body would not experience flutter at any finite speed. For the open tube the force and moment coefficients given by equations (14) and (15) were substituted into equations (1) and (2). In this case flutter speeds and frequencies did exist and the computed values are given in table 3 and are shown in figures 6 to 8.

For the tube on the faired struts the forces and moments given by equations (14) and (15) were used for the tube proper. For the fairing the force and moment were assumed to be given by two-dimensional theory at any section and were obtained from reference 4. The aerodynamic interaction between tube and fairing was thus neglected, as was the effect of the finite span on the forces experienced by the fairing. A Rayleigh-Ritz type of analysis was used with two modes, a linear torsion and a parabolic

bending mode. These modes were selected on the basis of the consideration that the struts deflect somewhat as shown in the two following schematic front views:



The flutter speeds and frequencies calculated in this manner are given in table 3 and are also shown in figure 8.

Calculation of the Frequency of the Uncoupled Yawing Oscillations

In order to determine what characteristics, if any, of the yawing-oscillation type of instability could be predicted, cognizance was taken of the fact that these oscillations did not involve any bending deflections; hence, h was set equal to zero in equations (1), (2), (9), and (10) and, for the sake of convenience, the structural damping coefficient was assumed to be zero as well. The following equations resulted:

$$\left\{ \omega^2 I_\alpha - K_\alpha + \rho v^2 L^3 \left[I_0 + 4k^2 (\sigma^2 I_0 - 2\sigma I_1 + I_2) \right] \right\} \alpha_0 = 0 \quad (18)$$

and

$$\left\{ \omega^2 m (s_2 - s_1) - \rho v^2 L^2 \left[2ikI_0 + 4k^2 (\sigma I_0 - I_1) \right] \right\} \alpha_o = 0 \quad (19)$$

A solution of equation (18) can be written as

$$f = f_\alpha \sqrt{\frac{1 - \frac{\rho v^2 L^3}{K_\alpha} I_0}{1 + \frac{\rho L^5}{I_\alpha} (\sigma^2 I_0 - 2\sigma I_1 + I_2)}} \quad (20)$$

This solution furnishes no information concerning a speed at which the oscillations may start but, instead, gives the frequency at which the body will tend to oscillate if it is yawed away from its equilibrium position and then released. This frequency is also the dominant frequency of the response of the body to random excitation. The term

$\frac{\rho L^5}{I_\alpha} (\sigma^2 I_0 - 2\sigma I_1 + I_2)$ in the denominator of the expression is the ratio of the moment of inertia of air at free-stream density contained within the body to the moment of inertia of the body alone, both taken about the elastic axis. This term is inversely proportional to the mass ratio; it depends on the shape of the body to some extent but is substantially independent of the elastic-axis location. Except at extremely low mass ratios, this term is negligibly small; for the airfoil-shaped body for instance, it is $0.0020 \frac{\rho}{\rho_o}$ and $0.0019 \frac{\rho}{\rho_o}$ for the elastic-axis location used in the tests of series I and II, respectively.

The numerator of the expression under the radical in equation (20) is equal to $1 - q^*$, where q^* is defined by

$$q^* = \frac{2qV_b}{K_\alpha} \quad (21)$$

Therefore, if the small term in the denominator is neglected, equation (20) can be written as

$$\frac{f}{f_{\alpha}} = \sqrt{1 - q^*} \quad (22)$$

In order to determine the speed at which these oscillations should occur equation (18) must be solved simultaneously with equation (19). However, the only real solution of equation (19) is $v = 0$ and, in addition, $x_{\alpha} = \frac{2\rho L^3}{m} (\sigma I_0 - I_1)$. Therefore, if the aerodynamic forces given by equations (9) and (10) were correct, oscillations could occur only at zero airspeed. These oscillations would then be the ordinary still-air yawing oscillations, the condition on x_{α} being that necessary to uncouple the yawing from the sidewise-bending mode.

Calculation of Divergence Speed

Inasmuch as divergence is a static instability phenomenon, the speed required to diverge the body can be found by setting h , ω , and q equal to zero in equations (1) and (10) or, more simply, setting $\omega = 0$ in equation (18). Thus,

$$\begin{aligned} v_{\text{divergence}} &= \sqrt{\frac{K_{\alpha}}{\rho L^3 I_0}} \\ &= \sqrt{\frac{K_{\alpha}}{\rho V_b}} \end{aligned} \quad (23)$$

or

$$q_{\text{divergence}} = \frac{K_{\alpha}}{2V_b} \quad (24)$$

The parameter q^* defined in equation (21) is thus equal to the ratio of q to $q_{\text{divergence}}$, the dynamic pressure at divergence being that calculated by using slender-body theory.

The divergence speeds for the tests of series VI and VII are given in table 3 and are shown in figures 7 and 8. For series I and II the value of $q_{\text{divergence}}$ may be obtained from equation (24), and for any

other test it can be obtained from the values of q^* and q given in table 3. Therefore,

$$\begin{aligned} q_{\text{divergence}} &= 1.97K_{\alpha} \text{ for series I and II} \\ &= 29.4 \text{ for series I} \\ &= 492 \text{ for series II} \\ &= \frac{q}{q^*}, \text{ in general} \end{aligned}$$

REFERENCES

1. Allen, H. Julian: Pressure Distribution and Some Effects of Viscosity on Slender Inclined Bodies of Revolution. NACA TN 2044, 1950.
2. Sewall, John L., and Woolston, Donald S.: Preliminary Experimental Investigation of Effects of Aerodynamic Shape of Concentrated Weights on Flutter of a Straight Cantilever Wing. NACA RM L9E17, 1949.
3. Gayman, William H.: An Investigation of the Effect of a Varying Tip Weight Distribution on the Flutter Characteristics of a Straight Wing. Jour. Aero. Sci., vol. 19, no. 5, May 1952, pp. 289-301.
4. Theodorsen, Theodore: General Theory of Aerodynamic Instability and the Mechanism of Flutter. NACA Rep. 496, 1935.
5. Smith, C. B., and Beane, Beverly J.: Damping in Pitch of Bodies of Revolution at Supersonic Speeds. Preprint No. 311, Inst. Aero. Sci., Feb. 1951.
6. Stewartson, K.: On Linearized Potential Theory of Unsteady Supersonic Motion. Quarterly Jour. Mech. and Appl. Math., vol. III, pt. 2, June 1950, pp. 182-199.
7. Von Kármán, Theodor: Calculation of Pressure Distribution on Airship Hulls. NACA TM 574, 1930.
8. Munk, Max M.: Aerodynamics of Airships. Vol. VI of Aerodynamic Theory, div. Q, W. F. Durand, ed., Julius Springer (Berlin), 1936, pp. 32-48.
9. Miles, John W.: On Non-Steady Motion of Slender Bodies. Aeronautical Quarterly, vol. II, pt. III, Nov. 1950, pp. 183-194.
10. Jones, Robert T.: Properties of Low-Aspect-Ratio Pointed Wings at Speeds Below and Above the Speed of Sound. NACA Rep. 835, 1946. (Supersedes NACA TN 1032.)

TABLE 1.- ORDINATES USED TO GENERATE
THE AIRFOIL-SHAPED BODY

s/L	R/L
0.005	0.0154
.0075	.0186
.0125	.0237
.025	.0315
.05	.0435
.075	.0529
.10	.0608
.15	.0732
.20	.0829
.25	.0901
.30	.0954
.35	.0985
.40	.0999
.45	.0993
.50	.0960
.55	.0906
.60	.0829
.65	.0736
.70	.0631
.75	.0516
.80	.0397
.85	.0277
.90	.0162
.95	.0061
1.00	0







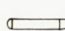


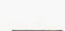


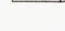
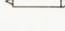
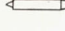
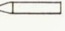
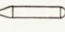
TABLE 2.- DIAMETERS AND EFFECTIVE SPRING
CONSTANTS OF STRUTS

Strut	Strut diameter, in.	K_h	K_α
A	0.040	10	20
B	.100	50	250
C	.166	110	430
D	.251	200	820



TABLE 3.- RESULTS OF AEROELASTIC-INSTABILITY TESTS

34

Body Nose Tail	Strut	m	I_{α}	a	x_{α}	f_h	f_{α}	Type of instability	$\rho \times 10^3$	v_{exp}	v_{anal}	q_{exp}	f_{exp}	f_{anal}	$\left(\frac{2v}{I_{\alpha} v}\right)_{exp}$	$\left(\frac{2v}{I_{\alpha} v}\right)_{anal}$	q^* q_{exp}
Test series I																	
	A	0.1301	0.0690	-0.28	0.10	1.20	2.82	Flutter	0.54	341	----	31.4	1.70	----	15.4	----	0.798
									.83	277	----	31.8	1.75	----	12.5	----	.808
									1.13	235	----	31.2	1.71	----	10.6	----	.793
									1.50	207	----	32.2	1.69	----	9.3	----	.818
									1.90	187	----	33.2	1.60	----	8.4	----	.834
									2.50	172	----	37.0	(a)	----	7.8	----	.940
Test series II																	
	B	0.1300	0.0670	-0.18	0	4.00	10.1	Yawing oscillation	2.33	299	----	104	9.25	8.99	3.76	----	0.210
									2.31	340	----	133	8.95	8.65	4.29	----	.269
									2.28	387	----	171	8.77	8.18	4.88	----	.345
									2.26	443	----	222	8.47	7.51	5.58	----	.448
									2.21	505	----	282	8.06	6.64	6.30	----	.569
									2.19	532	----	310	7.75	6.18	6.70	----	.626
Test series III																	
	B	0.1378	0.1014	-0.44	0.44	3.08	7.9	Yawing oscillation	2.28	234	----	62	7.5	----	3.84	----	0.276
	C	.1378	.1034	.24	-.24	4.03	10.2	Yawing oscillation	2.36	156-233	----	29	10.3-10.1	----	1.95-2.91	----	.075
	D	.1355	.1091	-.20	.20	5.85	14.4	Yawing oscillation	2.31	223-269	----	57	14.1-13.9	----	1.97-2.38	----	.077
	C	.1463	.1264	0	.06	4.18	9.2	Yawing oscillation	2.32	235-301	----	64	8.58-8.34	----	3.25-4.16	----	.181
	D	.1463	.1274	-.20	.26	5.61	12.9	None	2.22	479	----	254	4.73	----	----	----	.377
	C	.1635	.1626	0	.24	3.96	8.0	Yawing oscillation ^b	2.22	245-324	----	67	6.15	----	3.90-5.16	----	.190
	C	.1635	.1910	.44	-.20	4.11	7.5	Yawing oscillation ^b	2.21	435	----	209	(a)	----	7.39	----	.593
	C	.1392	.0904	0	-.04	4.34	10.9	Yawing oscillation ^b	2.05	312-412	----	109	(a)	----	3.65-4.82	----	.266
	D	.1392	.1045	-.20	.16	5.85	14.4	None	2.06	536	----	296	-----	----	4.75	----	.378
	D	.1383	.0926	-.20	.20	5.91	14.4	None	2.30	390	----	175	-----	----	3.45	----	.229
	D	.1394	.0950	-.20	.16	5.86	14.7	Yawing oscillation	2.24	223-256	----	56	14.7	----	1.93-2.22	----	.072
	D	.1348	.0926	-.20	.20	5.87	14.9	None	2.04	524	----	280	-----	----	4.48	----	.335
	C	.1677	.1630	.28	0	3.92	8.1	Yawing oscillation ^b	2.31	211-301	----	51	7.8	----	3.32-4.73	----	.137
	D	.1383	.0940	-.20	.20	5.90	14.8	Yawing oscillation	2.27	223-256	----	56	14.7-14.5	----	1.92-2.20	----	.073
	D	.1436	.1180	-.20	.30	5.65	13.2	None	2.21	368	----	150	-----	----	3.55	----	.215
	C	.1677	.1738	0	-.26	4.00	8.0	None	2.18	424	----	196	-----	----	6.75	----	.526
	C	.1635	.1766	0	-.24	3.92	7.8	Yawing oscillation	2.28	156-256	----	28	7.5-7.4	----	2.55-4.18	----	.079
	C	.1776	.2100	0	-.18	3.16	7.2	None	2.15	479	----	247	-----	----	8.48	----	.760

^aNot obtained.
^bIntermittent.

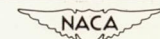
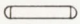





TABLE 3.- RESULTS OF AEROELASTIC-INSTABILITY TESTS - Concluded

Body Nose Tail	Strut	m	I_{α}	a	x_{α}	f_h	f_{α}	Type of instability	$\rho \times 10^3$	v_{exp}	v_{anal}	q_{exp}	f_{exp}	f_{anal}	$\left(\frac{2v}{I_{\alpha}\alpha}\right)_{exp}$	$\left(\frac{2v}{I_{\alpha}\alpha}\right)_{anal}$	q^*_{exp}
Test series IV																	
	C	0.1378	0.1301	0	0	4.35	10.6	Yawing oscillations	0.23	423	----	20.6	10.5	-----	5.07	-----	0.053
									.42	314	----	20.7	10.7	-----	3.78	-----	.054
									.61	233	----	16.6	10.5	-----	2.80	-----	.043
									.80	194	----	15.1	10.7	-----	2.34	-----	.039
									.99	171	----	14.5	10.4	-----	2.05	-----	.037
									1.19	160	----	15.2	10.7	-----	1.92	-----	.039
									1.38	160	----	17.7	10.7	-----	1.92	-----	.046
									1.57	162	----	20.6	10.7	-----	1.94	-----	.053
									1.77	152	----	20.5	10.6	-----	1.82	-----	.053
									1.96	158	----	24.4	10.6	-----	1.90	-----	.064
									2.15	145	----	22.6	10.6	-----	1.74	-----	.058
									2.31	129	----	19.2	10.4	-----	1.55	-----	.050
									Test series V								
	A	0.1410	0.0864	0	0.14	1.37	2.40	Flutter	0.55	195	140	10.5	1.51	1.99	10.32	7.42	0.516
									1.12	147	103	12.1	1.54	2.00	7.80	5.50	.594
									1.55	117	88	10.6	1.58	1.96	6.19	4.68	.521
									2.35	100	71	11.8	1.56	1.99	5.30	3.76	.579
Test series VI																	
	B	0.1237	0.0681	0	0	3.92	10.1	None	2.31	323	----	121	-----	-----	2.04	-----	0.471
		.1410	.0875	0	.08	3.10	8.4	Flutter	2.14	377	c ₂₉₆	152	(a)	6.8	5.71	4.48	.596
		.1410	.0708	0	0	3.11	9.2	Divergence	2.14	396	c ₃₁₂	168	-----	d _{7.3}	5.47	6.75	.659
		.1410	.0957	0	.14	3.07	8.2	Flutter	2.14	369	c ₃₀₄	146	5.50	6.7	5.73	4.72	.573
		.1580	.1217	0	.26	3.01	7.4	Flutter	2.14	353	c ₃₂₃	133	(a)	6.1	6.06	5.56	.522
		.1750	.1475	0	.36	2.81	7.0	Flutter	2.14	331	c ₃₅₁	117	4.60	5.6	6.00	6.38	.459
		.1580	.1217	0	0	3.00	7.3	Flutter	2.14	389	c ₂₇₆	162	(a)	6.2	6.78	4.82	.636
		.1750	.1475	0	-.14	2.83	6.8	Divergence	2.14	424	e ₁₇₇	192	-----	d _{6.6}	7.95	9.13	.754
		.1580	.1217	0	-.26	2.96	7.5	Divergence	2.14	375	c ₁₂₄	150	-----	d _{8.0}	6.37	8.28	.589
		Test series VII															
	e _B	0.1410	0.0708	0	0	5.41	13.7	Divergence	2.14	522	284	292	-----	-----	4.86	2.64	1.146
		.1410	.0708	0	0	5.41	13.7	Flutter and divergence	2.14	481	f ₁₃₅	248	-----	d _{4.7}	4.48	81.25	.974
		.1410	.0875	0	.08	5.30	13.0	Flutter	2.14	486	f ₁₁₃	253	(a)	3.9	4.51	1.11	.993
		.1580	.1217	0	-.26	3.40	11.1	Divergence	2.14	427	f ₂₂₁	195	-----	d _{3.3}	4.90	3.26	.766
		.1750	.1475	0	-.14	2.97	8.1	Divergence	2.14	393	f ₉₉	165	-----	d _{2.1}	6.16	4.46	.648
		.1750	.1475	0	.36	2.87	8.1	Flutter	2.14	332	f ₆₁	118	4.30	2.0	5.20	.96	.463

^aNot obtained.

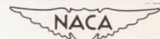
^cCalculated flutter speed; the calculated divergence speed is 487.

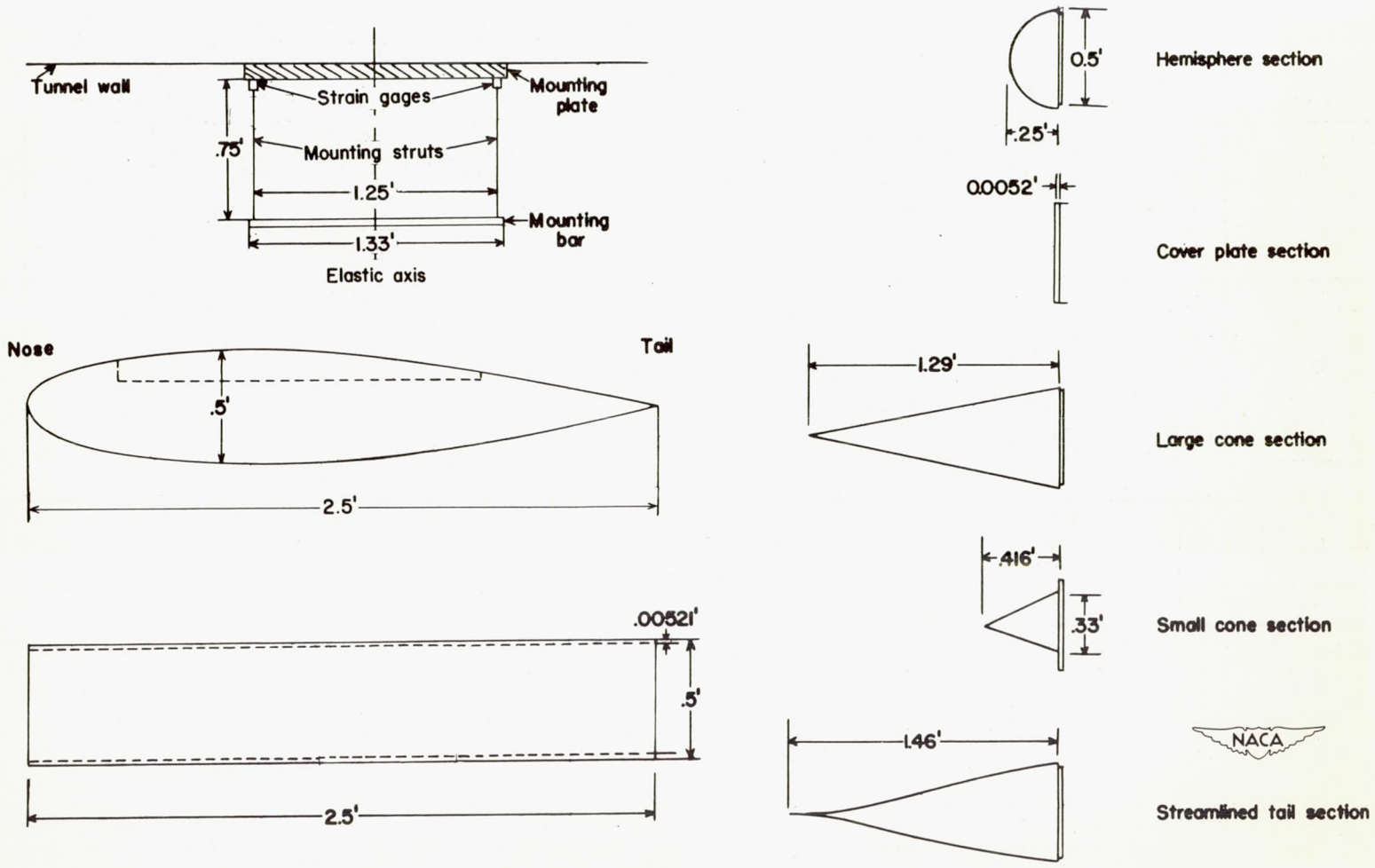
^dCalculated flutter frequency.

^eStruts covered with fairing simulating thin airfoil.

^fCalculated flutter speed; the calculated divergence speed is 284.

^gBased on calculated flutter speed.

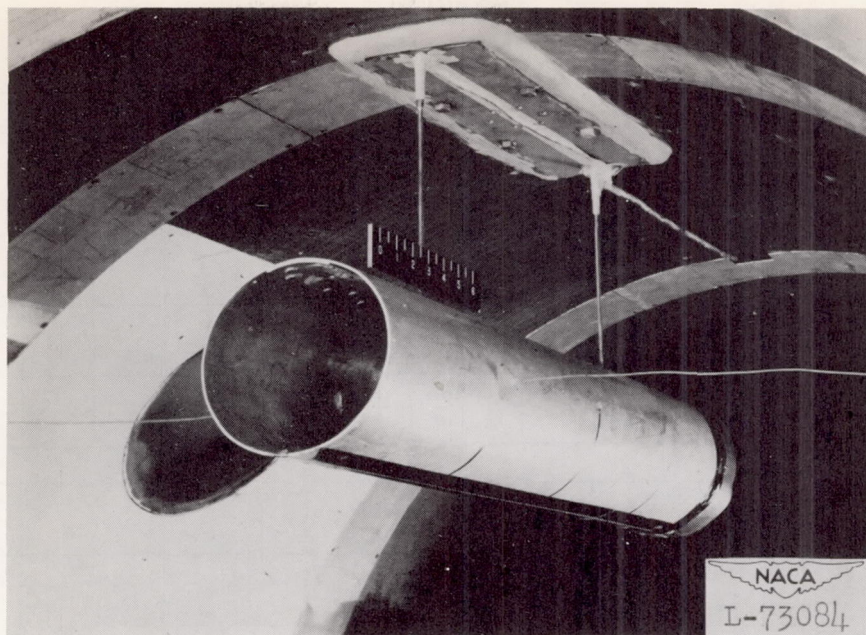




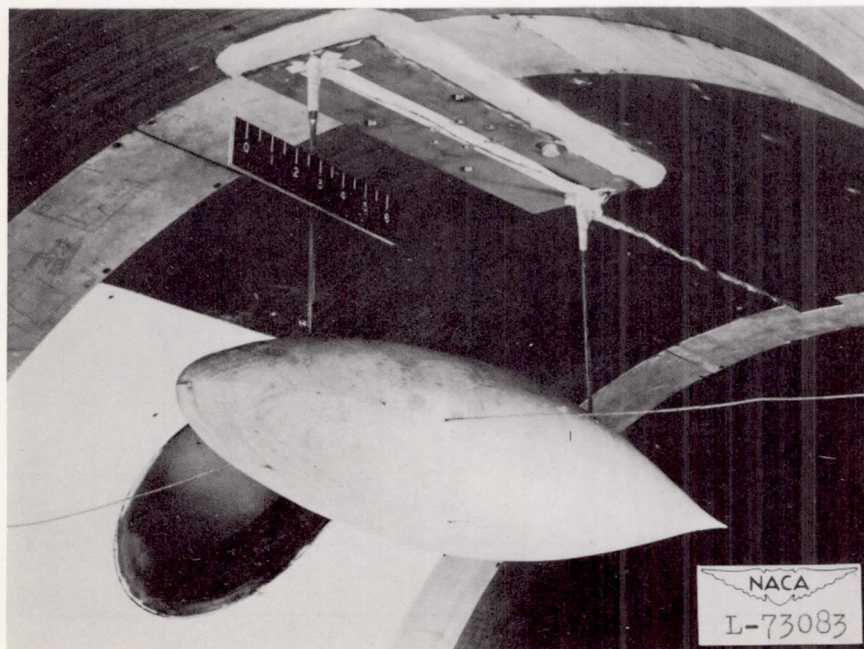
(a) Airfoil-shaped body, basic open tube, and supports.

(b) Bodies of revolution used as nose and tail sections for the basic tube.

Figure 1.- Dimensions of the various bodies and the support system.



(a) Open tube.



(b) Airfoil-shaped body.

Figure 2.- Models mounted in the Langley 4.5-foot flutter research tunnel.

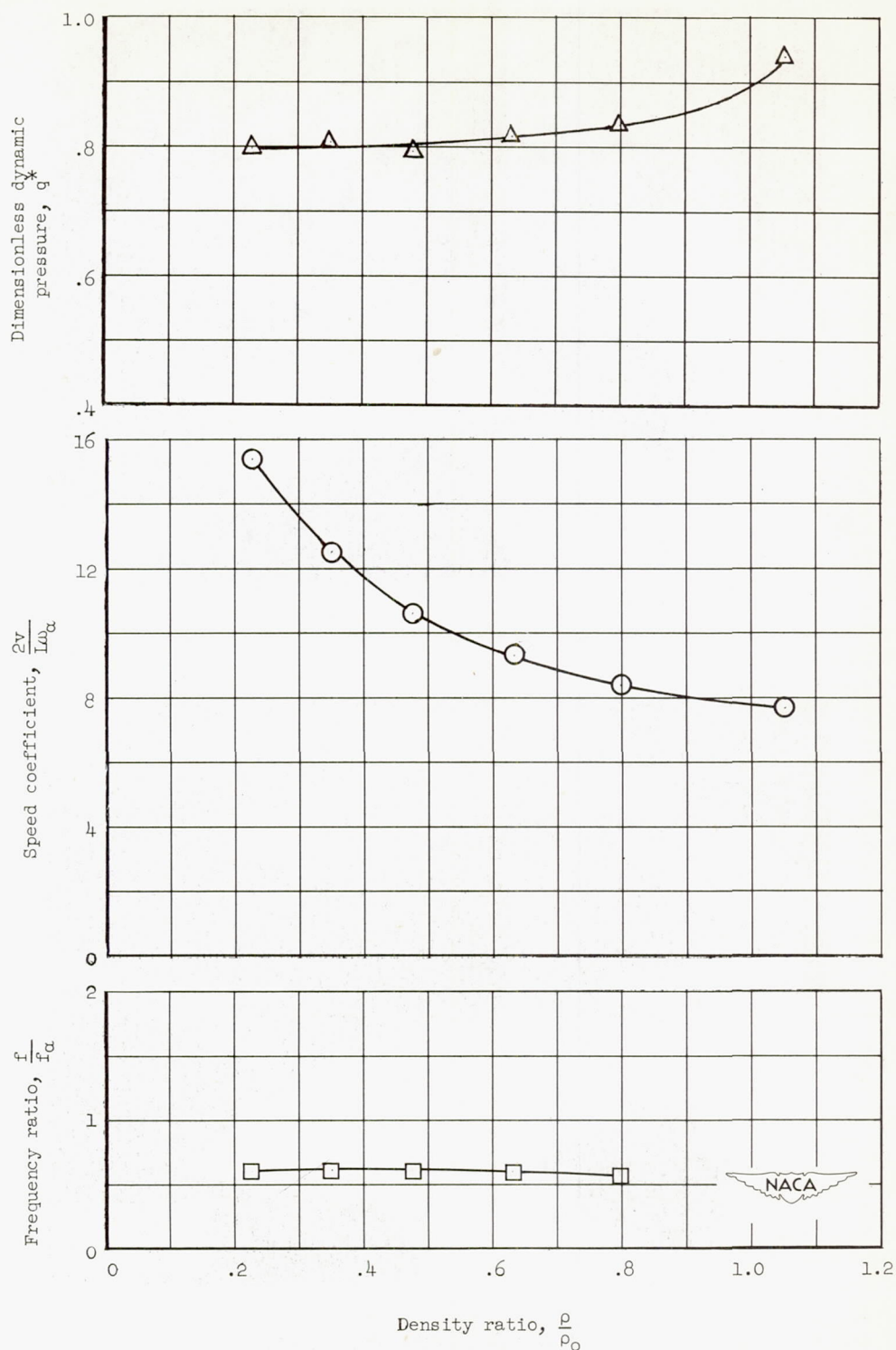


Figure 3.- Plot of experimental speed, dynamic-pressure, and frequency parameters at flutter for the airfoil-shaped body. (Table 3, test series I.)

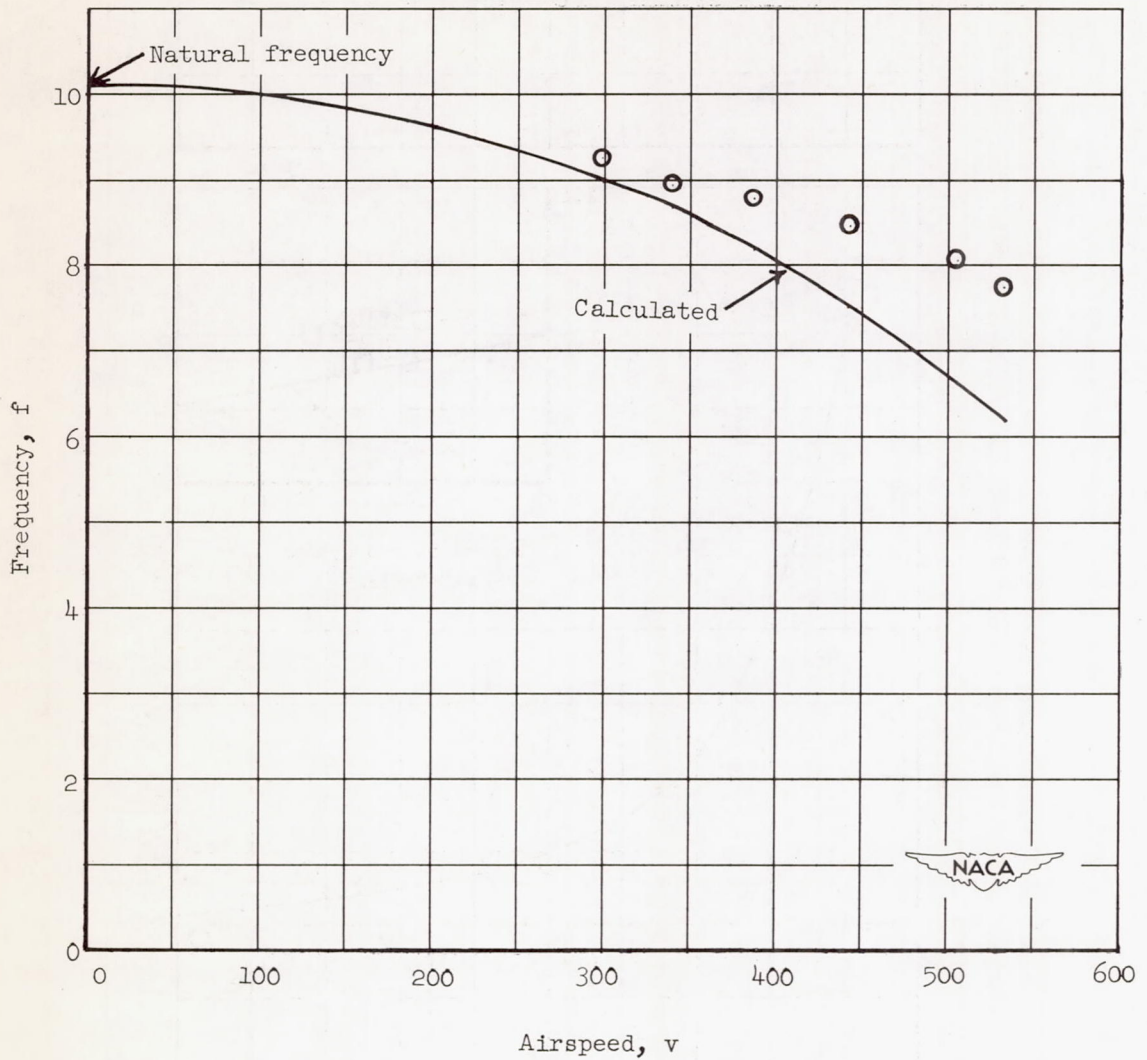


Figure 4.- Plot of frequency of yawing oscillations against airspeed for the airfoil-shaped body. (Table 3, test series II.)

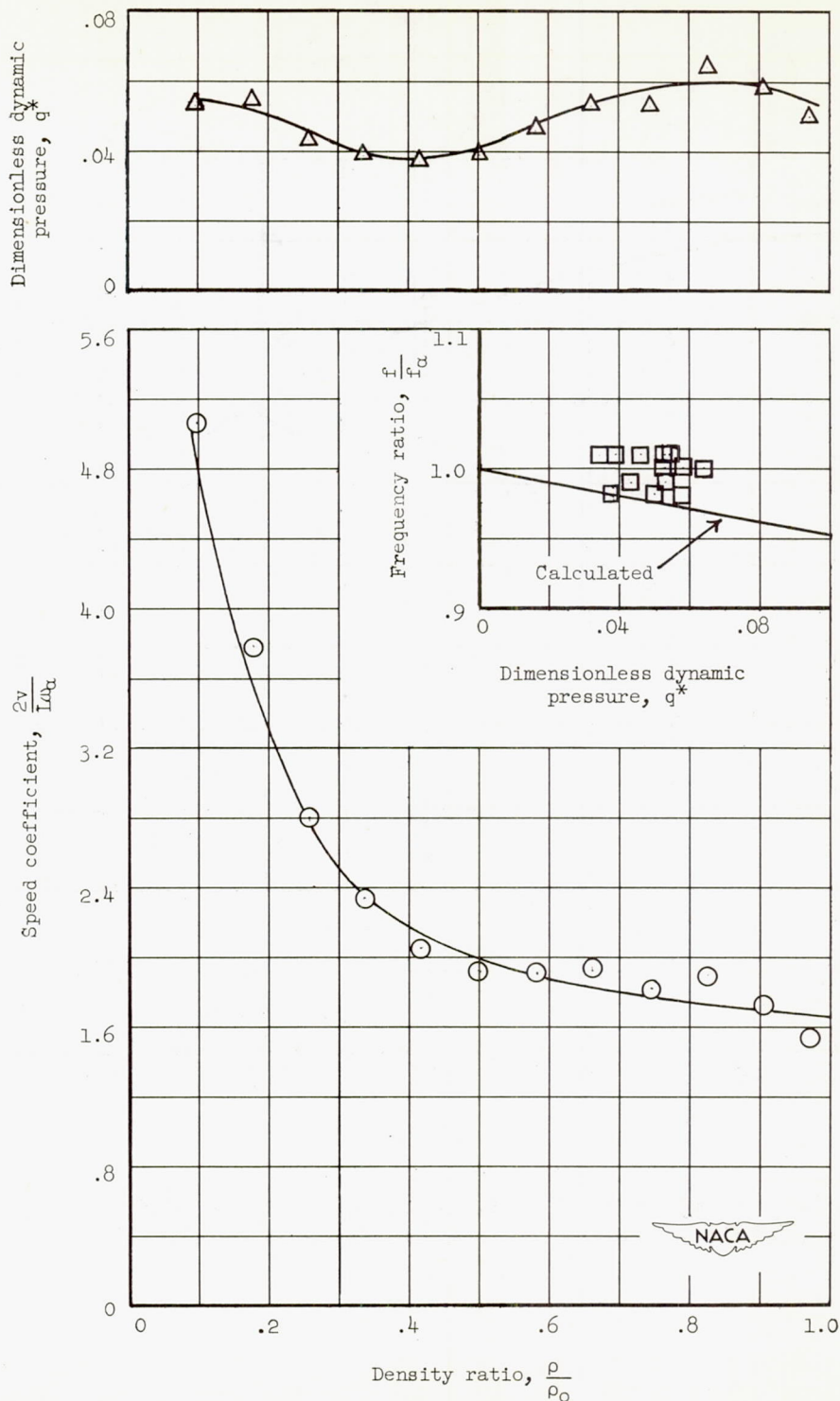


Figure 5.- Plot of speed coefficient and dimensionless dynamic pressure against the density ratio for the body with hemispherical nose and tail. (Table 3, test series IV.)

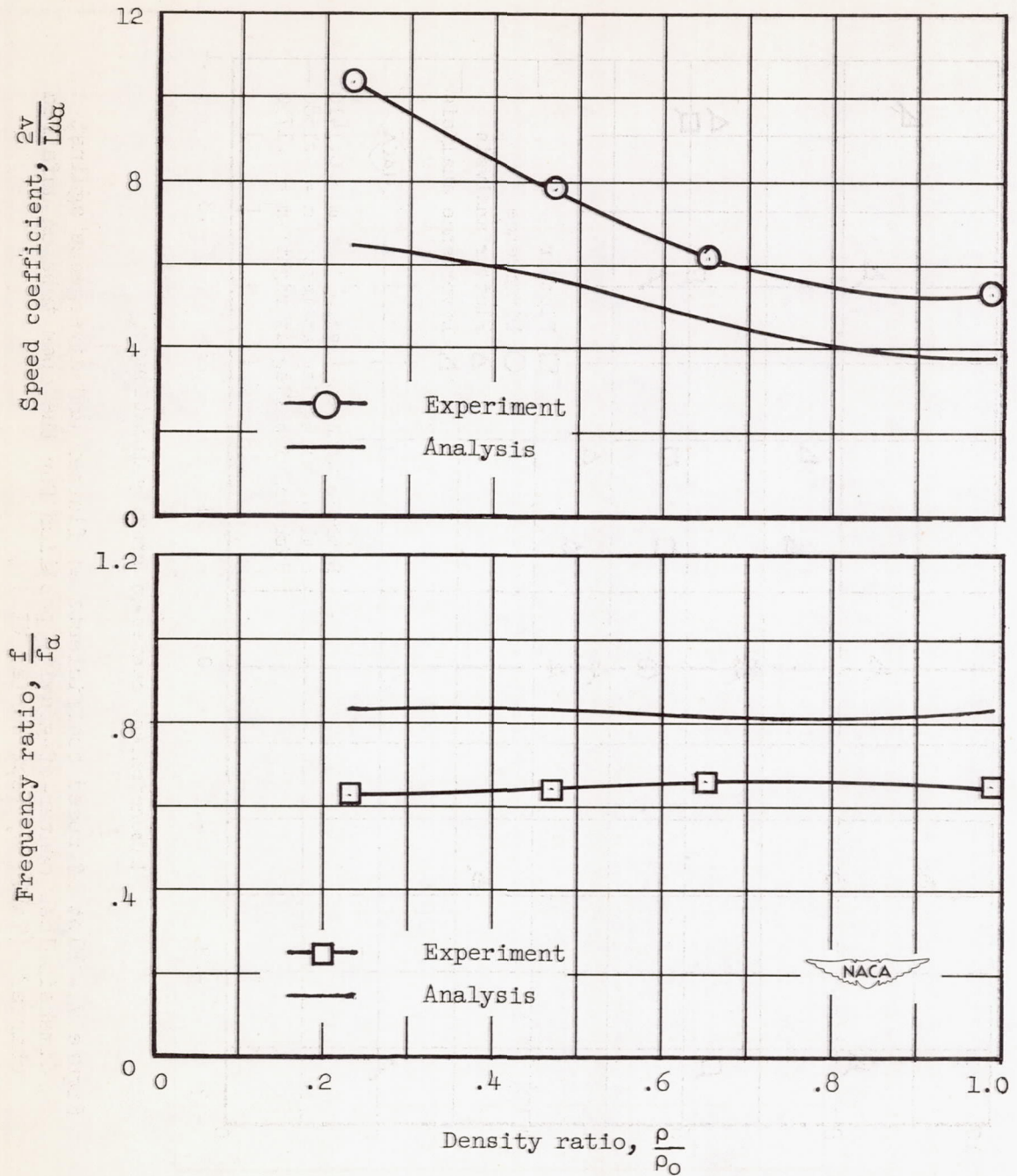


Figure 6.- Plot of experimental and analytical speed and frequency parameters against the density ratio for the open tube. (Table 3, test series V.)

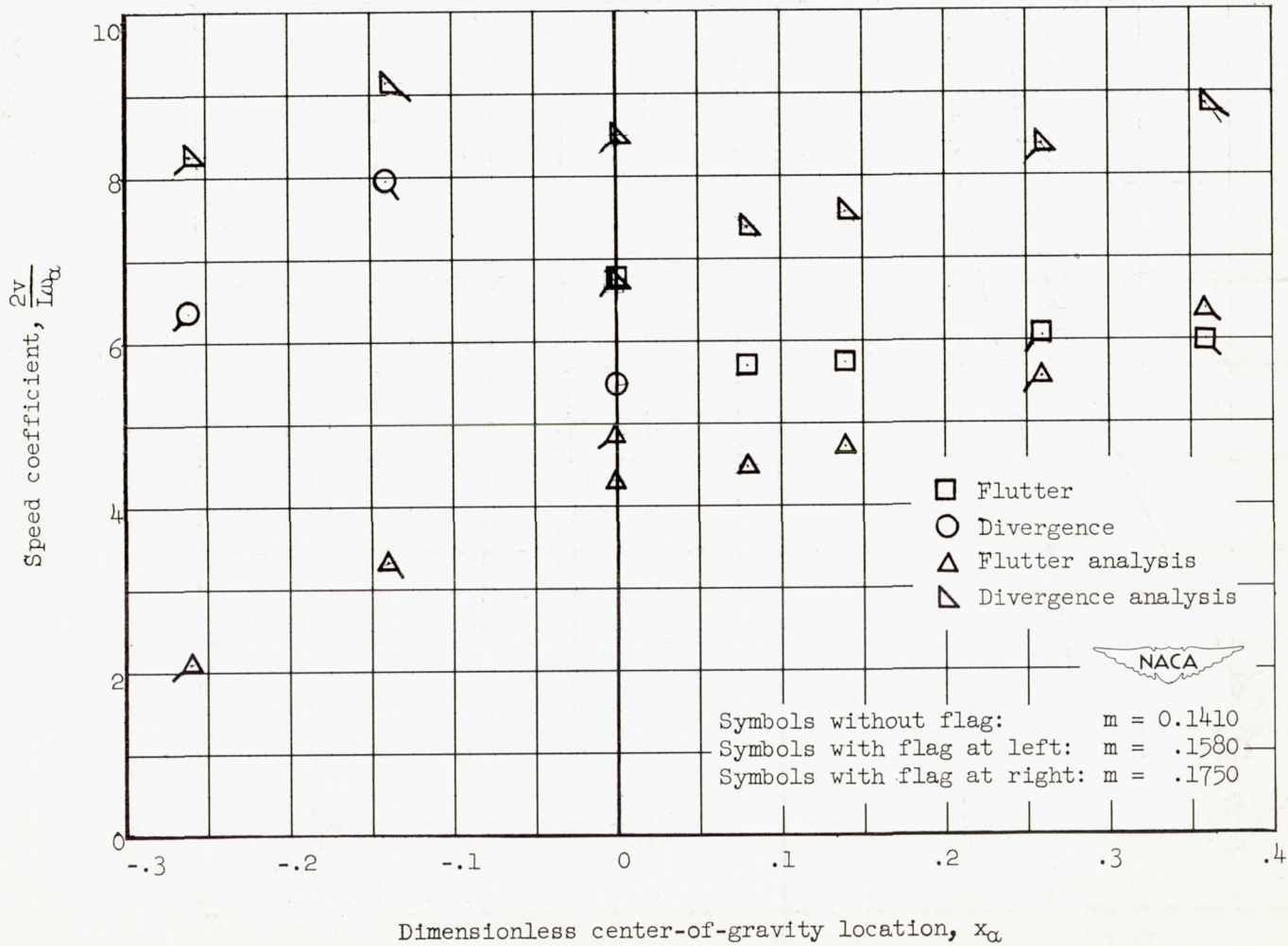


Figure 7.- Plot of speed coefficients at flutter and divergence against dimensionless center-of-gravity position for the open tube on unfaired charts. (Table 3, test series VI.)

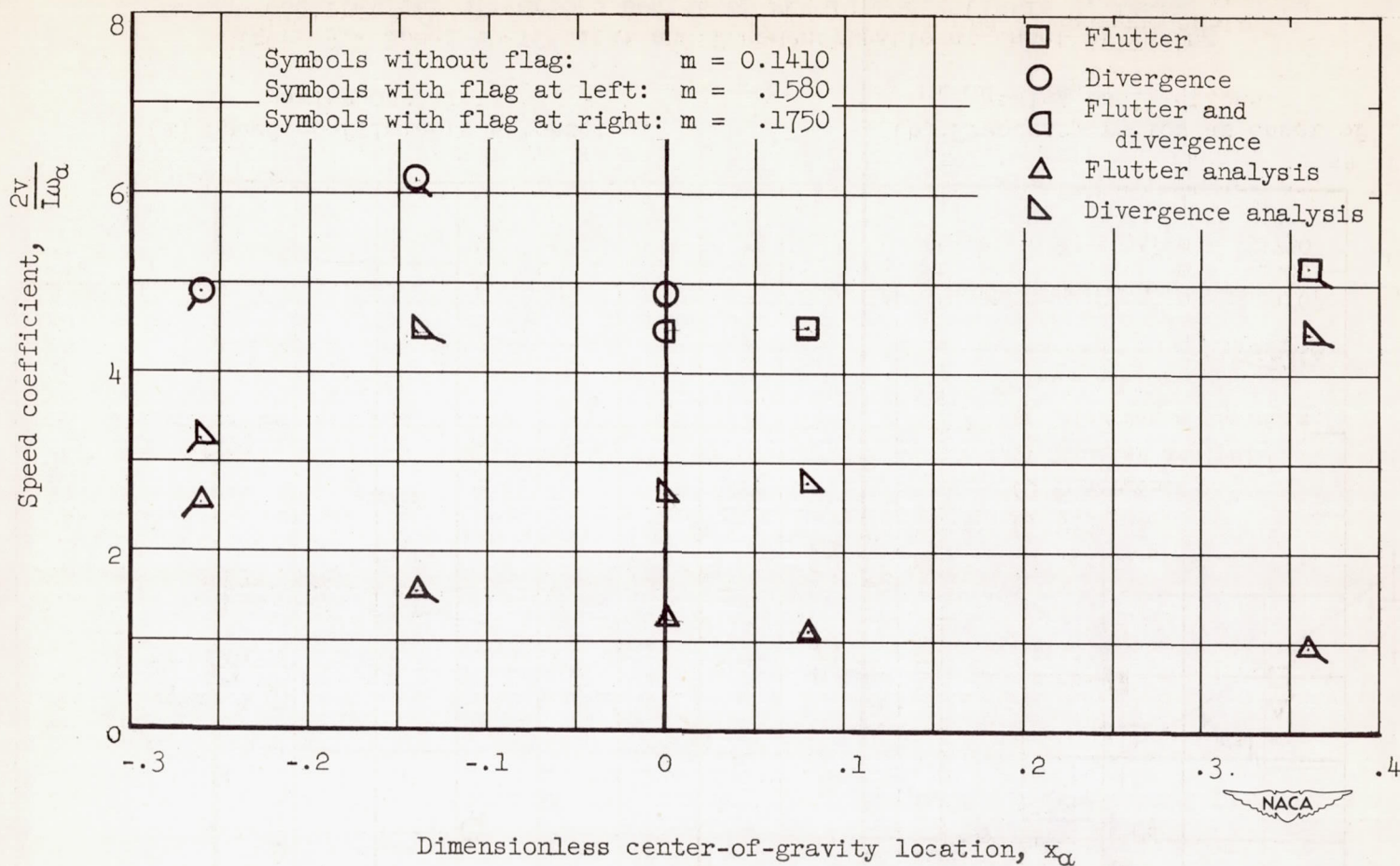
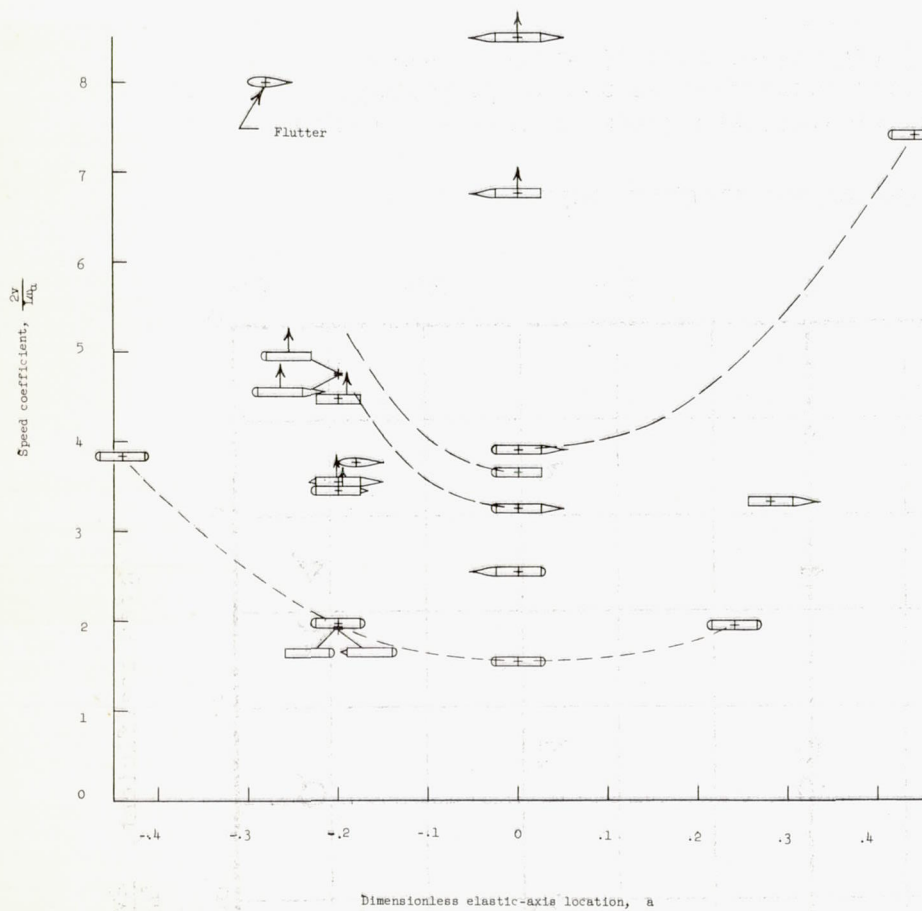
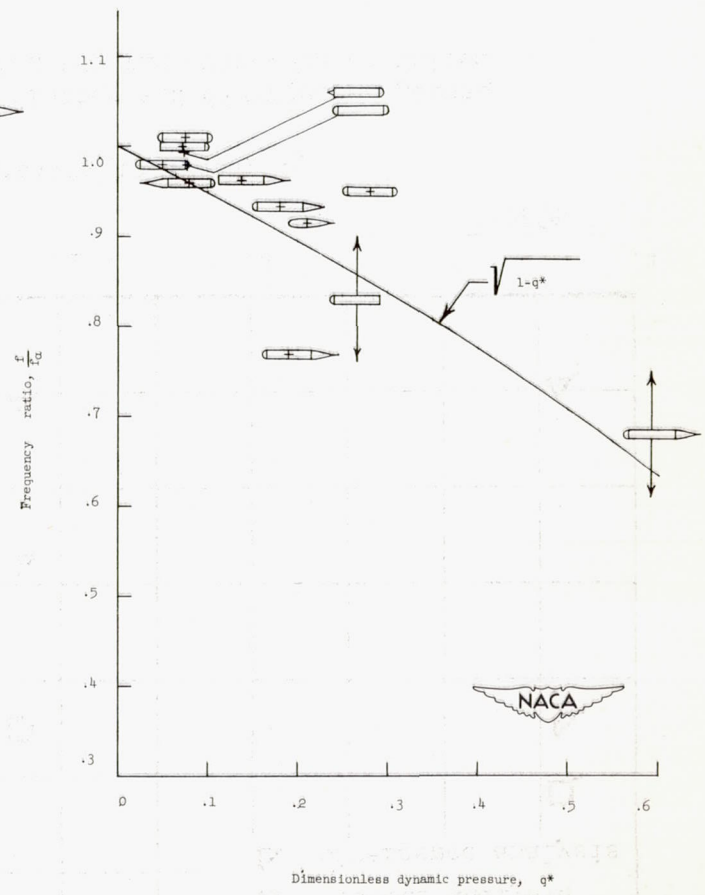


Figure 8.- Plot of speed coefficients at flutter and divergence against dimensionless center-of-gravity position for the open tube on faired charts. (Table 3, test series VII.)



(a) Speed coefficients at onset of yawing oscillations.



(b) Frequency ratios at onset of yawing oscillations.

Figure 9.- Speed coefficient and frequency ratio at onset of yawing oscillations of various bodies of revolution. (Table 3, test series III.)